Solvent Effects on Ground and Excited Electronic State Structures of the Push-Pull Chromophore Julolidinyl-*n*-*N*,*N*′-diethylthiobarbituric Acid

Andrew M. Moran, Claire Delbecque,† and Anne Myers Kelley*

Department of Chemistry, Kansas State University, Manhattan, Kansas 66506-3701

Received: May 2, 2001; In Final Form: August 29, 2001

Resonance Raman spectra and cross sections of a "push−pull" chromophore containing a julolidine donor and a thiobarbituric acid acceptor have been measured in dilute solution in five solvents having a wide range of polarities (cyclohexane, 1,4-dioxane, dichloromethane, acetonitrile, and methanol) at excitation wavelengths spanning the strong visible charge-transfer absorption band. The absolute Raman excitation profiles and absorption spectra are simulated using time-dependent wave packet propagation techniques to determine the excited-state geometry changes along the ∼30 Raman-active vibrations as well as the solvent reorganization energies. Several vibrational modes undergo significant (5−15 cm^{-1}) frequency changes as the solvent is varied, signaling solvent polarity effects on the ground-state electronic structure. The excited-state geometry changes are solvent dependent for some vibrational modes but not for others. The total vibrational reorganization energy decreases, and the solvent reorganization energy increases with increasing solvent polarity in all solvents except the one protic solvent, methanol, which is anomalous in both respects. Tentative assignments are made for the ground-state vibrational modes by comparison of the Raman frequencies and infrared frequencies and intensities with those calculated using density functional theory, as well as by comparison with model compounds. The results are discussed within the context of the two-state valence-bond model for the electronic properties of conjugated push−pull chromophores.

Introduction

"Push−pull" chromophores possess an electron-donating group and an electron-accepting group connected by a conjugated pi system. There is particular interest in the rational design of such chromophores to maximize their often large nonlinear polarizabilities, both the first hyperpolarizability β and the second hyperpolarizability γ.[1−12] The nonlinear optical properties of such chromophores are often discussed by invoking two-state valence-bond models for the ground and first excited electronic states.[5,13−21] Although these models are conceptually useful, the few quantitative tests of their predictions against results from experiments or higher levels of theory have produced mixed results.[13,15,18,22] We recently tested predictions of the two-state valence-bond model for the effect of solvent polarity on the ground- and excited-state geometries of the prototypical push−pull chromophore, *p*-nitroaniline (PNA).[23] Here we extend these studies to the more complicated but also more highly nonlinear chromophore shown in Figure 1, julolidinyl-*n*-*N*,*N*′-diethylthiobarbituric acid[3,24] (subsequently referred to as JTB). The corresponding compound having six conjugated bonds linking the donor and acceptor has one of the largest β values ever measured.[5]

Figure 1 indicates resonance between neutral and zwitterionic structures whose interconversion involves interchanging double and single bonds. Two-state valence-bond models take these two structures as basis states whose linear combinations constitute the two lowest-energy electronic eigenstates. If, as in many push−pull molecules, the ground state is predominantly the neutral form and the lowest excited state predominantly the zwitterion, the lowest-energy electronic transition corresponds to an intramolecular charge-transfer excitation. The resulting large change in dipole moment upon excitation leads to strong solvatochromism: in PNA, for example, the absorption maximum red-shifts by 4000 cm^{-1} as the solvent is varied from cyclohexane to methanol. The two-state valence bond model also predicts that the description of the ground and excited adiabatic electronic states should vary with solvent polarity. This is because polar solvents lower the energy of the zwitterionic state more than that of the neutral state, bringing them closer together in energy and causing them to mix more in the true adiabatic eigenstates. Thus, with increasing solvent polarity the ground and excited states should become more nearly equal mixtures of the basis states and should have more similar equilibrium geometries, resulting in a smaller internal vibrational reorganization energy upon electronic excitation. We found this prediction to hold qualitatively for PNA, but the solvent effect on the ground state (as evidenced by the vibrational frequencies) appeared to be much smaller than the effect on the excited-state structure (manifested in the ground- to excited-state geometry changes).[23] We concluded that the two-state mixing model does not tell the whole story.

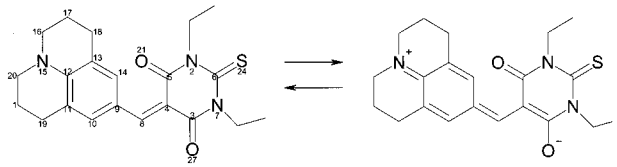

Figure 1. Neutral and zwitterionic structures of JTB showing the numbering of the heavy atoms.

In this paper, we report resonance Raman spectra and absolute excitation profiles for JTB in five solvents: cyclohexane (nonpolar), dioxane (weakly polar), dichloromethane (more

* To whom correspondence should be addressed. E−mail: amkelley@ksu.edu.

† Current address: Ecole Nationale Supérieure de Chimie de Clermont Ferrand, Aubière, France.

10.1021/jp011662t CCC: $20.00
Published on Web 10/16/2001

polar), acetonitrile (highly polar but nonprotic), and methanol (highly polar and hydrogen-bonding). JTB was chosen for several reasons: it has a rather large first hyperpolarizability β_0 of 50×10^{-30} esu in chloroform[24] (about a factor of 5 larger than that for PNA[25]), it has a very strong absorption in the visible region of the spectrum, and unlike the longer polyenic members of the series,[5,24] it does not have the complication of possible cis−trans isomerism. The vibrational frequencies allow us to assess the solvent dependence of the ground-state electronic structure. Simulation of the optical absorption spectra and resonance Raman excitation profiles provides the solvent reorganization energies and the changes in geometry along each ground-state normal coordinate from which we can deduce the solvent effects on the excited-state structure.

Experimental and Computational Methods

JTB was synthesized via the Knoevenagel condensation of 9-julolidine-carboxaldehyde and 1,3-diethyl-2-thiobarbituric acid.[24] The julolidine carboxaldehyde was first prepared by Vilsmeier−Haack−Arnold acylation of julolidine (Aldrich) with DMF in the presence of $POCl_3$.[26,27] The aldehyde was recrystallized twice from ethanol/water and used quickly in the second step of the synthesis. Reaction of the aldehyde with 1,3-diethyl-2-thiobarbituric acid (Aldrich) yielded the product JTB as a fluffy pink solid in 60−90% yield. The NMR and optical absorption spectra were in good agreement with those reported in ref 24.

Solutions of JTB were prepared in methanol, acetonitrile, dichloromethane, 1,4-dioxane, and cyclohexane (Fisher certified, spectroscopic, or HPLC grades). Molar extinction coefficients for the visible charge-transfer transition in the five solvents were determined relative to that reported in chloroform (104 000 M^{-1} cm^{-1} at 524 nm)[24] by obtaining spectra of equal dilutions of a common stock solution into each of the five solvents. All absorption spectra were measured on a Hitachi U-3010 UV−visible spectrophotometer. The molar extinction coefficient ϵ (L mol^{-1} cm^{-1}) is related to the absorption cross section σ_A (cm^2 $molecule^{-1}$) by

$$\sigma_A = 10^3 \ln(10)\epsilon/N_A \quad (1)$$

where N_A is Avogadro's number.

The infrared spectrum of JTB was obtained as a KBr pellet on a Nicolet Protege 460 FTIR spectrometer.

Resonance Raman spectra of JTB were acquired using the 457.9, 476.5, 488.0, 496.5, 501.7, and 514.5 nm lines from a cw argon-ion laser (Lexel model 95-4). Excitation at 532 nm was obtained from a frequency-doubled diode-pumped cw Nd:YVO_4 laser (Millennia Vs), 545 and 551 nm were generated from an argon-ion-pumped dye laser (Spectra-Physics 375B) operating with Coumarin 540, and 569 nm was obtained from the dye laser with Rhodamine 590. Excitation wavelengths of 424.2 and 632.8 nm, used only in the solvent cross section calibrations, were provided by a frequency-doubled picosecond mode-locked Ti:sapphire laser (Spectra-Physics Tsunami) and a He−Ne laser, respectively. For the resonance Raman experiments, the incident beam of about 3.5 mW power was focused onto about 2 mL of sample contained in a rotating quartz cell. Solutions were prepared in the 20−30 μM range. The actual concentration used in each experiment was determined spectrophotometrically, and spectra were obtained both before and after data collection to ensure that no thermal or photochemical degradation had occurred. The Raman scattering was collected in a backscattering geometry with aluminum coated ellipsoidal and flat mirrors and passed through a polarization scrambler before being dispersed by a Spex 1877 triple spectrograph and detected with a Spex Spectrum One liquid-nitrogen-cooled CCD detector. The slit width at the entrance to the spectrograph stage was 100 μm, giving a spectral resolution of about 5−6 cm^{-1} depending on excitation wavelength.

A total of 8−20 accumulations of 20−120 s each were added at each setting of the spectrograph. The frequency axis was calibrated using known solvent lines. Intensities were corrected for the wavelength dependence of the collection and detection system using an Optronic Laboratories 245C tungsten−halogen lamp, and the intensities were corrected for reabsorption in our backscattering geometry. Band areas were determined using the GRAMS/32 (Galactic Industries) curve-fitting algorithm to fit mixed Gaussian/Lorentzian peak profiles.

Differential cross sections ($d\sigma_R/d\Omega$) for JTB were calculated relative to the cross sections for solvent lines (cyclohexane 801 cm^{-1}, dioxane 835 cm^{-1}, dichloromethane 702/740 cm^{-1} doublet, acetonitrile 919 cm^{-1}, methanol 1035 cm^{-1}) by

$$\left(\frac{d\sigma_R}{d\Omega}\right)_u = \frac{I_u}{I_v}\frac{c_v}{c_u}\left(\frac{d\sigma_R}{d\Omega}\right)_v \quad (2)$$

where "u" and "v" denote solute and solvent, respectively, I is the measured integrated band intensity, and c is the concentration in the neat liquid. Absolute Raman cross sections for the other four solvents were determined relative to the 801 cm^{-1} line of cyclohexane as an external standard.[28] The cyclohexane cross sections were assumed to obey an A-term dependence

$$(d\sigma_R/d\Omega) = K\upsilon_0(\upsilon_0 - \upsilon_v)^3[(\upsilon_e^2 + \upsilon_0^2)/(\upsilon_e^2 - \upsilon_0^2)^2]^2 \quad (3)$$

where υ_0 is the laser excitation wavenumber in cm^{-1}, υ_v is the Raman shift of the vibration, υ_e is the wavenumber of the resonant state, and K is a prefactor that scales the overall cross sections. The A-term parameters of Trulson and Mathies, obtained by fitting to total absolute cross section data over the wavelength range 647 to 239 nm, were employed. The prefactor was converted from total to differential cross section by using the relation

$$\left(\frac{d\sigma_R}{d\Omega}\right) = \frac{3}{8\pi}\frac{1+\rho}{1+2\rho}\sigma_{R,total} \quad (4)$$

where ρ is the depolarization ratio, taken to be 0.08 for the 801 cm^{-1} cyclohexane line.

The resonance Raman intensities and absorption spectra were modeled using the time-dependent formalism described in detail elsewhere.[28,29] The resonance Raman differential cross section is calculated as

$$\frac{d\sigma_R}{d\Omega} = \sum_i B_i \sum_f \int d\omega_S \times \left[\frac{\omega_S^3\omega_L}{c^4}\int_{-\infty}^{\infty} d\delta\, G(\delta)\frac{4}{15}\left|\alpha_{if}(\omega_L, \delta)\right|^2\right] L_{if}(\omega_L - \omega_S) \quad (5)$$

where B_i is the Boltzmann population of initial vibrational state i, ω_L and ω_S are the incident and scattered laser frequencies, respectively, $G(\delta)$ is an inhomogeneous distribution of solvent-induced electronic frequency shifts δ assumed here to be a Gaussian of standard deviation θ, L_{if} is the normalized line shape of the $i \rightarrow f$ ground-state vibrational transition, and the integral

TABLE 1: A-term Fitting Parameters for Solvent Raman Cross Sections

parameter	methanol	acetonitrile	dichloromethane	dioxane	cyclohexane
ν_v/cm^{-1}	1035	919	702/740[a]	835	801
K/Å^2 sr^{-1}	7.62×10^{-11}	8.99×10^{-12}	1.92×10^{-10} (vis) 1.34×10^{-11} (UV)	4.41×10^{-11}	9.99×10^{-11}
ν_e/cm^{-1}	153 100	105 700	126 900 (vis) 74 800 (UV)	99 600	115 000

[a] Parameters refer to the 702 cm^{-1} line alone in the UV region and the combined 702/740 cm^{-1} doublet in the visible region.

over ω_S extends over the range of a given Raman band. The Raman polarizability, α_{if}, is given by

$$\alpha_{if}(\omega_L, \delta) = \frac{|\mu_0|^2}{\hbar}\int_0^\infty dt\, \langle\chi_f|\chi_i(t)\rangle \exp[i(\omega_L - \omega_0 - \delta + \omega_i)t - g(t) - \Gamma t/\hbar] \quad (6)$$

where μ_0 is the electronic transition moment evaluated at the ground-state equilibrium geometry, $|\chi_i\rangle$ and $|\chi_f\rangle$ are the initial and final vibrational wave functions multiplied by the coordinate-dependent transition dipole moment, e.g.

$$|\chi_i\rangle = \sum_r [(\partial\mu/\partial q_r)/\mu_0] q_r |i\rangle \quad (7)$$

where the sum is over all vibrational normal modes, $|\chi_i(t)> = \exp(-iHt/\hbar)|\chi_i\rangle$ is this initial state propagated on the excited-state potential surface for time t, ω_0 is the electronic zero-zero frequency, $g(t)$ is a solvent broadening function (see below), and Γ is the line width due to electronic population relaxation or other exponentially decaying processes. The corresponding optical absorption cross section is given by

$$\sigma_A(\omega) = \frac{4\pi|\mu_0|^2\omega}{3n\hbar c}\sum_i B_i \int_{-\infty}^{\infty} d\delta\, G(\delta)\, \mathrm{Re}\int_0^\infty dt\, \langle\chi_i|\chi_i(t)\rangle \exp[i(\omega - \omega_0 - \delta + \omega_i)t - g(t) - \Gamma t/\hbar] \quad (8)$$

where n is the solvent refractive index.

Each of the vibrational modes observed to have significant intensity on resonance was modeled as a pair of harmonic surfaces with equal ground- and excited-state frequencies and potential minima displaced by a distance Δ in dimensionless normal coordinates.[30] The ground- and excited-state frequencies were assumed to be equal, as the simulated data are not very sensitive to moderate changes in excited-state frequency (when Δ is nonzero) and this parameter cannot be determined accurately. The shapes of the excitation profiles are, however, quite sensitive to any vibrational coordinate dependence of the transition dipole moment, and we found it necessary to include a small linear coordinate dependence for a few modes. The solvent was modeled as a single Brownian oscillator in the overdamped limit.[31,32] A small amount of static inhomogeneous broadening was also included as a Gaussian distribution of zero−zero energies, although the quality of the fits was not very sensitive to this parameter. We also found that the fits to the absorption spectra in particular were greatly improved by adding a modest amount of pure exponential broadening (100−175 cm^{-1}). Thermal population of the three lowest quantum levels of each of the three vibrational fundamentals below 420 cm^{-1} (a total of 27 distinct initial states) was incorporated in the modeling.

A ground-state geometry optimization and vibrational frequency calculation was performed with the B3LYP hybrid density functional and the 6-311G** basis set using Gaussian 98 (Gaussian, Inc).[33] Normal modes were viewed with Molden 2.6.

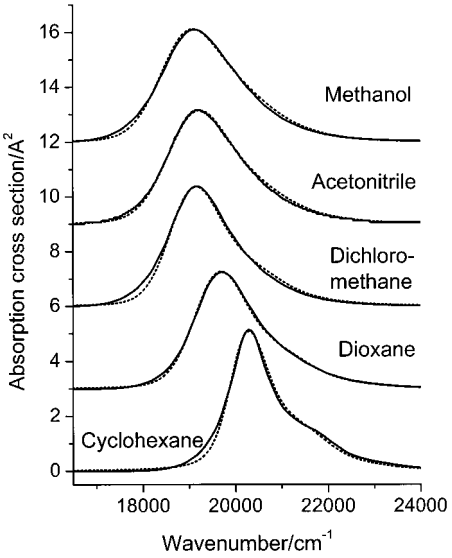

Figure 2. Absorption spectra of JTB in the indicated solvents (solid curves) and spectra calculated from the parameters of Table 4 (dashed curves). Successive spectra are vertically offset by 2 Å^2.

Results

A. Absolute Raman Cross Sections for Solvent Standards. Table 1 gives the A-term fitting parameters for each of the five solvents used in the resonance Raman experiments. The parameters for cyclohexane are taken from ref 34 as described in the Methods section. The parameters for the other four solvents were obtained by fitting the cross sections measured relative to cyclohexane at 296, 325, 360, 404, 424, 476, 514, and 633 nm. The data in methanol, acetonitrile, and dioxane were fit acceptably well to a single A-term over the full wavelength range. The data in dichloromethane could not be fit to a single A-term over this range; the cross sections exhibit almost no preresonance enhancement between 360 and 633 nm and then rise sharply to the UV. Therefore, the data for this solvent alone were fit to two different A-terms, a "visible" function covering the region from 360 to 633 nm and a UV function over the region 296−360 nm. These A-term parameters were then used to generate a best value for the solvent cross sections at each of the excitation wavelengths from which the absolute Raman cross sections for JTB were calculated using eq 2.

B. Absorption Spectra. Figure 2 shows the absorption spectra of JTB in cyclohexane, dioxane, dichloromethane, acetonitrile, and methanol. The spectrum in cyclohexane has a band shape typical of large molecules with weak Franck−Condon activity: a strong, fairly sharp feature attributable to the electronic origin plus weak progressions in low-frequency vibrations, and a weaker feature to the blue arising from mostly 0−1 vibronic bands of the higher-frequency modes. This structure is washed out by solvent broadening in the more polar solvents. The spectrum red-shifts strongly on going from nonpolar cyclohexane (λ_{max} = 493 nm) to more polar solvents, but

TABLE 2: Absorption Maxima of JTB and Solvent Properties

solvent	cyclohexane	1,4-dioxane	dichloro-methane	acetonitrile	methanol
λ_{max}/nm	493	507	522	521	523
ϵ^a	2.0	2.2	9.1	37.5	32.6
n_D^{20} [a]	1.43	1.42	1.42	1.34	1.33
ET(30)[b]	30.9	36.0	40.7	45.6	55.4

[a] Reference 35. [b] Reference 36.

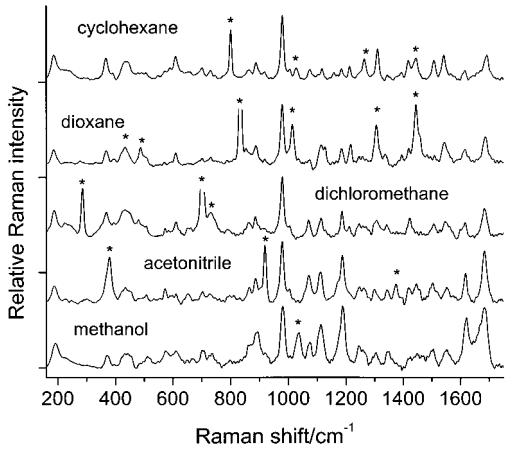

Figure 3. Resonance Raman spectra of JTB in the indicated solvents. Excitation wavelengths are 476.5 nm for cyclohexane, 496.5 nm for dioxane, and 514.5 nm for the other three solvents. Fluorescence backgrounds have been subtracted. All spectra have been scaled to have approximately equal intensities in the strong 979 cm^{-1} line. The offset of the *y* axes is arbitrary. Asterisks mark lines due primarily to solvent.

interestingly, the absorption maximum is nearly constant at 521−523 nm in dichloromethane, acetonitrile, and methanol. Dichloromethane is much less polar (lower dielectric constant) than acetonitrile and methanol but is considerably more polarizable (higher refractive index). The integrated intensity of the absorption does not vary much among solvents, but the maximum extinction coefficient decreases as the spectrum broadens in the more polar solvents. Table 2 summarizes the absorption spectral data as well as measures of solvent polarity and polarizability for the five solvents employed.

C. Resonance Raman Spectra. Figure 3 presents representative resonance Raman spectra of JTB in the five solvents excited near the absorption maximum in each solvent. In each case, the Raman lines were superimposed on a substantial fluorescence background, typically 5−10 times stronger than the strongest Raman line. This background was fit to a polynomial and subtracted prior to band integration and presentation of the data. Excitation on the blue side of the absorption band yielded resonance Raman spectra of much higher quality due to the reduced fluorescence background. All of the observed lines are believed to correspond to vibrational fundamentals; a few lines at frequencies above the range plotted here are probably attributable to overtones and combination bands, but these are extremely weak because of the small Δ values (vide infra). The number of Raman lines actually observed varied from 21 to 30 in different solvents, mainly because the intensities of the weaker lines could not be determined accurately when there was strong overlap with a solvent band.

To allow qualitative comparison of intensities, the spectra in Figure 3 have been plotted such that the strong 979 cm^{-1} line is about the same intensity in each solvent. It is immediately apparent that the relative intensities of many lines are quite solvent dependent. The strong lines near 1185, 1622, and (to a lesser extent) 1689 cm^{-1} all gain relative intensity as the solvent polarity increases from top to bottom in the figure. The lines near 1308 and 1550 cm^{-1}, in contrast, become considerably less pronounced as the solvent polarity is increased. The Raman lines are also somewhat broader in the more polar solvents, particularly in methanol.

TABLE 3: Resonance Raman Frequencies for JTB in Five Solvents

Raman shift/cm^{-1}				
cyclohexane	dioxane	dichloromethane	acetonitrile	methanol
186	187	187	187	180−192[a]
229	227	226	227	222
366	370	368	*b*	365
b	*b*	421	425	433
439	444	445	447	*c*
c	*b*	495	495	500
c	569	573	573	571
c	*c*	*c*	590	*c*
611	611	611	611	604
c	697	*b*	701	698
725	730	*b*	729	727
b	*b*	*b*	793	*c*
b	*b*	862	863	863
889	886	887	886	887
917	917	917	*b*	906
979	979	979	979	979
996	*b*	*c*	1004	*b*
1075	1072	1071	1072	*b*
1104	*b*	1103	1103	1105
1117	*b*	1113	1113	1116
b	*b*	*b*	1168	1169
1184	1185	1185	1185	1187
1212	*b*	*c*	1213	1215
b	1246	1244	1247	1246
b	1263	*c*	1264	1266
1310	1313	1303	1308	1306
b	*b*	1343	1348	1347
1388	*b*	*c*	*b*	*b*
1417	1419	*b*	1421	1421
1506	*c*	1503	1506	1506
1540	1542	1547	1552	1556
1616	1613	1614	1622	1622
1666	*c*	*c*	*c*	*c*
1691	1687	1684	1689	1685

[a] Frequency is excitation wavelength dependent; it varies from 180 cm^{-1} in the blue (476 nm excitation) to 192 cm^{-1} in the red (551 nm excitation). [b] Not clearly observed due to nearly solvent lines. [c] Too weak to be clearly observed even though there is no significant solvent intensity in that region.

Table 3 gives the frequencies of the resonance Raman lines in all five solvents. Shifts of more than 2 cm^{-1} in strong lines or 4 cm^{-1} in weak ones should be considered significant. Most of the vibrational frequencies vary weakly if at all with solvent, but a few of them show some solvent dependence. In particular, the line at 1540 cm^{-1} in cyclohexane shifts to progressively higher frequencies with increasing solvent polarity, reaching 1556 cm^{-1} in methanol. In general the frequencies in methanol tend to be anomalous, particularly for the lower-frequency lines; for example, the sharp line at 611 cm^{-1}, whose frequency is constant to within 1 cm^{-1} in the other four solvents, appears at 604 cm^{-1} in methanol, and the line at 917 cm^{-1} in cyclohexane, dioxane, and methylene chloride, obscured by a strong solvent line in acetonitrile, drops to 906 cm^{-1} in methanol. Also, the line around 187 cm^{-1} exhibits a fairly strong excitation wavelength dependence of its vibrational frequency in methanol, ranging from 180 to 181 cm^{-1} in the blue (476−496 nm excitation) to 190−192 cm^{-1} in the red (545−551 nm excitation). This is the only line that shows a significantly excitation wavelength-dependent vibrational frequency in any solvent.

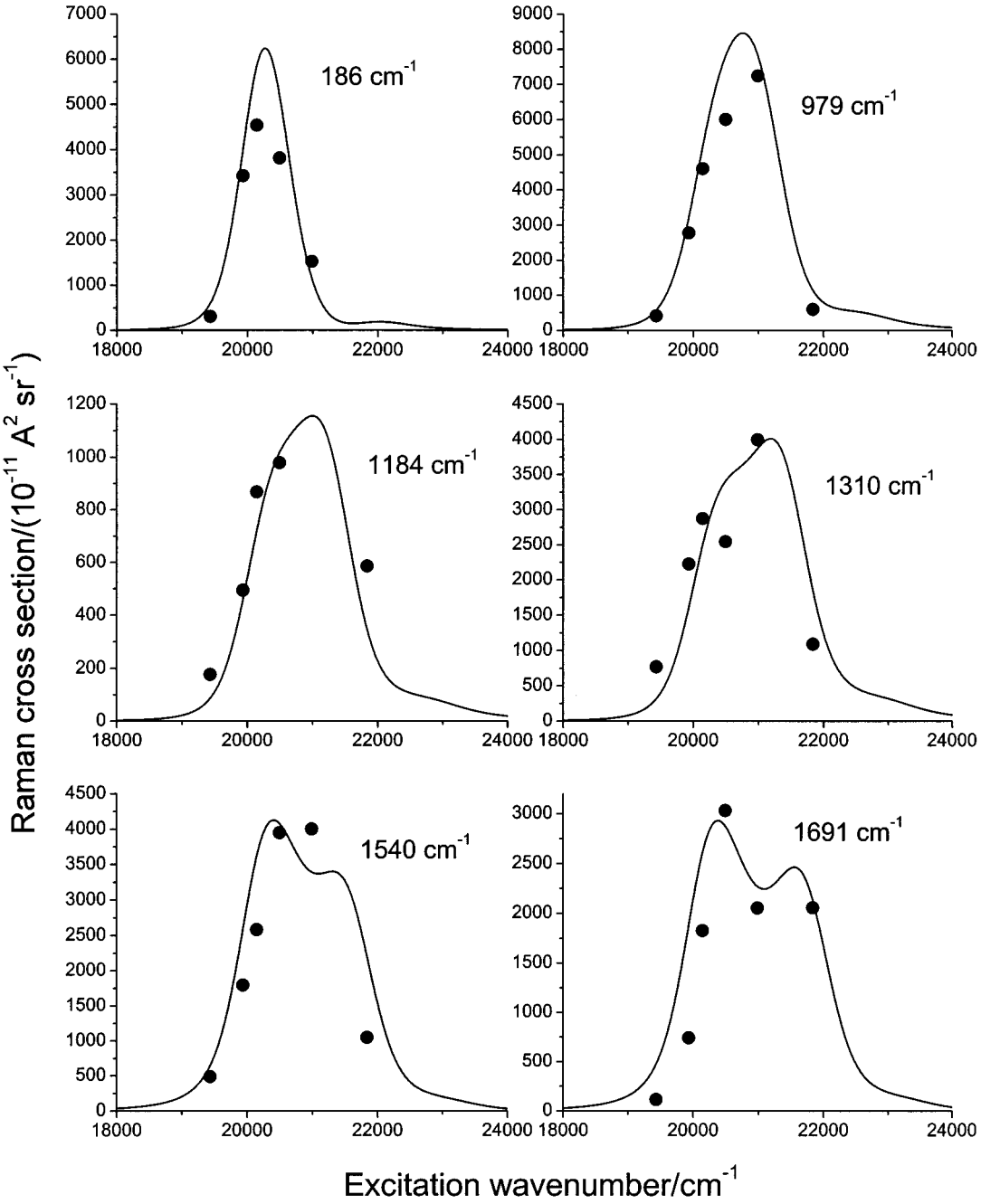

Figure 4. Experimental (points) and calculated (lines) resonance Raman excitation profiles for JTB in cyclohexane. The calculated profiles are generated from the parameters of Table 4.

D. Modeling of Absorption Spectra and Resonance Raman Profiles. In each solvent, the absorption spectrum and the excitation profiles for each of the observed Raman lines were simultaneously fit to a model for the ground and excited-state potential energy surfaces and spectral broadening parameters as described in the Methods section. Figure 2 shows the calculated fits to the absorption spectra in all five solvents, whereas Figures 4−6 show the fits to the excitation profiles for six fundamentals in three of the solvents. Table 4 summarizes the fitting parameters in each of the five solvents.

The parameters that best fit the full excitation profiles and absorption spectra reveal some differences from the qualitative conclusions that might have been reached by examination of Figure 3, which displays the spectra at a single excitation wavelength. The displacements in the 1689 and 1622 cm^{-1} modes are actually fairly constant in the four more polar solvents, although smaller in cyclohexane. The 1185 cm^{-1} mode shows an increased Δ in the more polar solvents, whereas the displacements in the 1308 and 1550 cm^{-1} modes decrease substantially with increasing solvent polarity. With the exception of methanol, the total resonance Raman intensity decreases as the solvent polarity increases. As a result, the overall scaling of the displacements has to be smaller and the solvent reorganization energy larger in the polar solvents in order to simultaneously recover the correct absorption band shape and the resonance Raman intensities. Again excluding methanol, the fitting parameters show a smooth trend toward decreasing total vibrational reorganization energy and increasing solvent reorganization energy as solvent polarity increases. Figure 7 summarizes the frequencies and displacements for four modes as a function of ET(30) solvent polarity scale, capturing the range of solvent dependences (or their lack) exhibited by different modes.

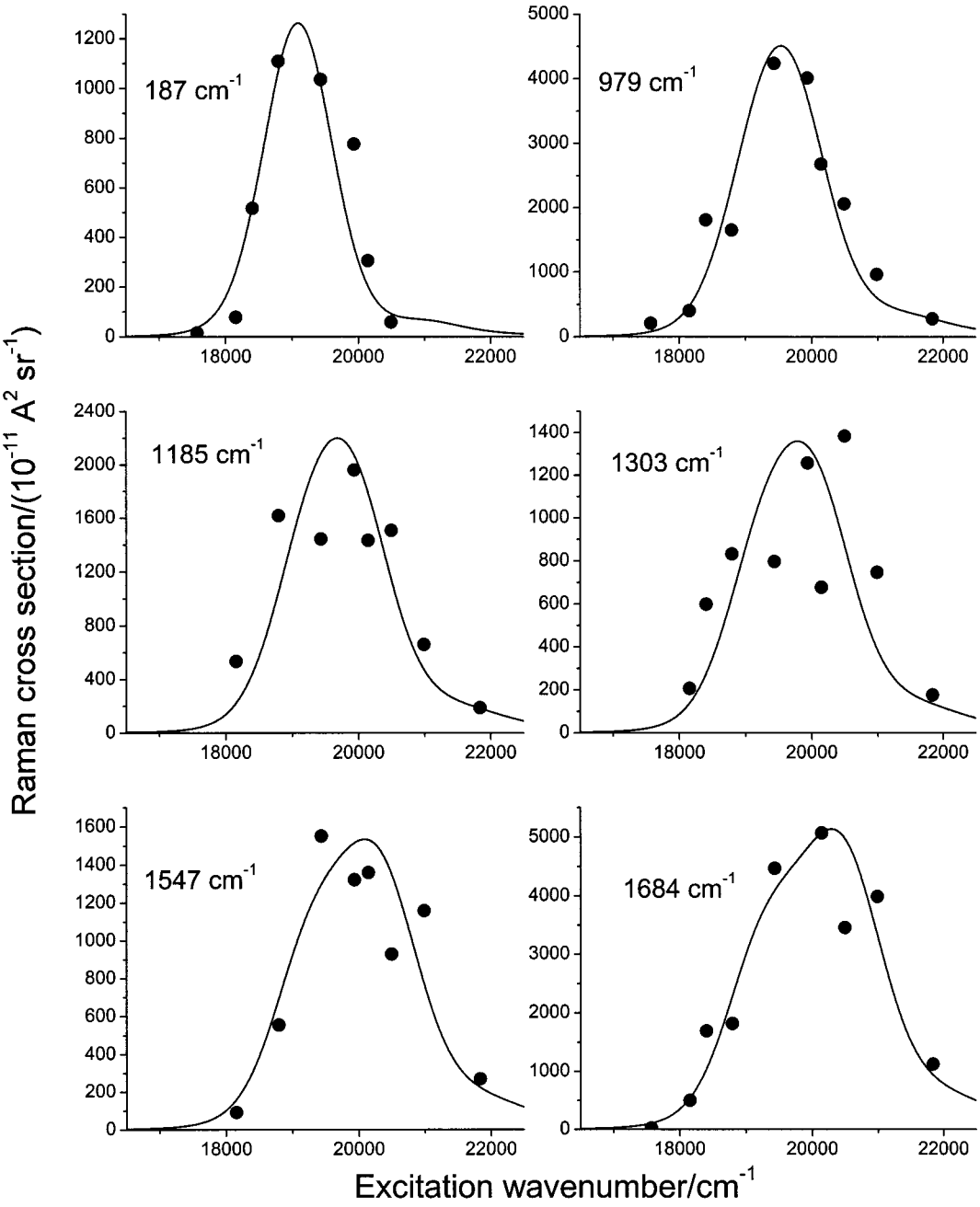

Figure 5. Same as Figure 4, in dichloromethane.

As was seen with the vibrational frequencies, the fitting parameters in methanol appear somewhat anomalous. The overall absolute resonance Raman intensities are considerably larger in methanol than in the other polar solvents, requiring larger displacements and a smaller solvent reorganization energy in methanol. The total reorganization energy ($\lambda_v + \lambda_s$) increases smoothly from 692 cm^{-1} in cyclohexane to 1269 cm^{-1} in acetonitrile but then drops to 900 cm^{-1} in methanol.

E. Ground-State Normal Modes and Excited-State Geometries. The ground-state vibrational frequencies observed in the resonance Raman spectra were tentatively assigned to calculated normal modes as summarized in Table 5. These assignments were made by comparison of experimental and calculated frequencies, comparison of experimental and calculated infrared intensities, and the qualitative consideration that the strongly resonance Raman-active modes should be largely in-plane vibrations with high local symmetry. In a few cases, we also made use of the experimental nonresonant Raman spectra of the acceptor (1,3-dithiobarbituric acid)[37] and the donor (julolidine)[38] alone, as well as the resonance Raman spectra of julolidinemalononitrile, the analogous push−pull molecule bearing a julolidine donor and a dicyanovinyl acceptor.[39]

A few comments should be made about these assignments. The generally lower vibrational frequencies of the IR bands relative to the Raman bands is due at least in part to a matrix effect, solution versus microcrystalline. The KBr pellets were too fluorescent to give adequate Raman spectra, but we were able to discern a few strong lines at 1547, 1493, 1308, 1254, 1114, 1073, and 980 cm^{-1}. The predominantly ethylenic C═C stretching mode, calculated at 1571 cm^{-1}, is predicted to be intense in the infrared, but we observe no IR intensity between 1499 and 1612 cm^{-1}. We assign the strong Raman mode near 1546 cm^{-1} as this predominantly ethylenic stretch despite its lack of IR activity. The alternative is to assign the 1616 cm^{-1}

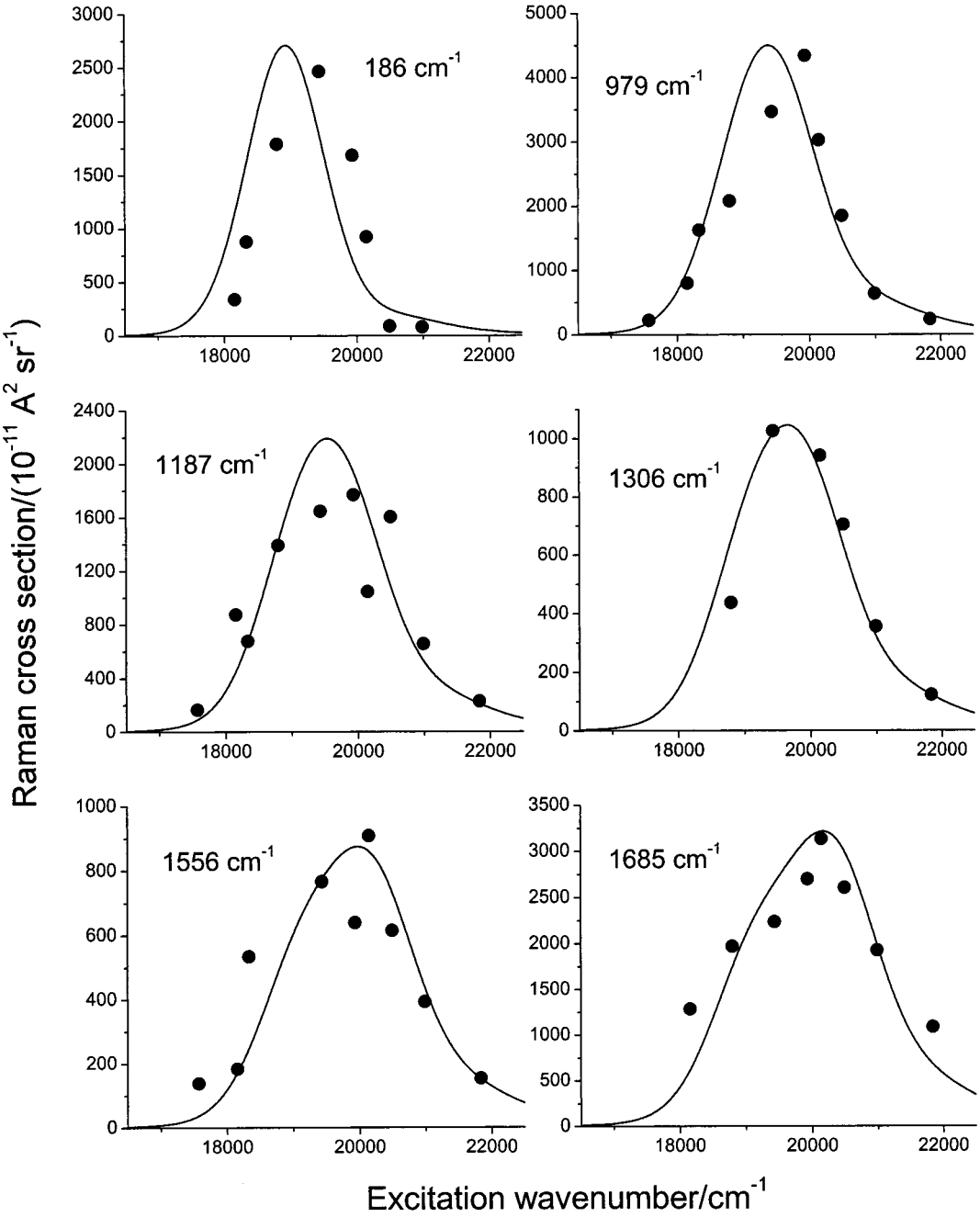

Figure 6. Same as Figure 4, in methanol.

Raman/1612 cm^{-1} IR band to the C═C stretch and the 1546 cm^{-1} Raman line to the "quinoidal" stretching mode of the julolidine moiety calculated at 1651 cm^{-1}, but this would assume a large error in the calculated frequency ordering and appears less likely based on other criteria explored in the Discussion section. The assignments of the low-frequency lines are also problematic. The assignment of the observed strong Raman line at 187 cm^{-1} to the mode calculated at 184 cm^{-1}, a delocalized bending vibration that leads to an overall long-axis in-plane expansion, seems quite solid. The equivalent mode is strongly Franck−Condon active in most conjugated polyenes and aromatic molecules. However, there are no predominantly in-plane modes calculated between 184 and 326 cm^{-1}. The calculated modes closest in frequency to the observed 227 cm^{-1} line are methyl torsions, which are unlikely to be resonance Raman enhanced. We therefore prefer to assign the 227 cm^{-1} line to the next highest frequency in-plane mode, largely an NCS bend, even though its calculated frequency is much higher. Most of the other assignments, while quite plausible, are by no means unique or definitive.

Discussion

We recently completed a similar study on a simpler prototypical push−pull molecule, *p*-nitroaniline (PNA).[23] In that work, we not only obtained solvent-dependent ground-state frequencies and excited-state dimensionless displacements along the Franck−Condon active normal modes but also converted the Δ values into actual excited-state bond length and bond angle changes. That level of detail about the excited-state geometry is not obtainable for JTB for a combination of two reasons: the uncertainty in assigning observed frequencies to ground-state normal modes and the indeterminacy in the signs of the experimentally determined dimensionless displacements. The

TABLE 4: Spectral Simulation Parameters for JTB in Five Solvents[a]

solvent	cyclohexane	1,4-dioxane	dichloromethane	acetonitrile	methanol
electronic inhomog. std. dev. (θ)/cm^{-1}	0	290	0	0	400
classical reorg. energy (λ_s)/cm^{-1}	162	294	536	884	289
electronic lifetime broadening (Γ)/cm^{-1}	175	125	100	100	100
electronic origin (ω_0)/cm^{-1}	20000	19245	18500	18275	18525
transition length/Å	2.469	2.522	2.555	2.574	2.59
vib. freq. (ω)/cm^{-1} [b]	Δ, ($\partial\mu/\partial$q)/μ_0				
187	0.8, 0	0.738, 0	0.587, 0	0.47, 0	0.825, 0
227	0.42, 0	0.322, 0	0.354, 0	0.234, 0	0.478, 0
368	0.44, 0	0.42, 0	0.264, 0		0.255, 0
425			0.263, 0	0.152, 0	0.483, 0
447	0.42, 0	0.216, 0	0.275, 0	0.226, 0	
495			0.186, 0	0.154, 0	0.18, 0
573		0.194, 0	0.179, 0	0.112, 0	0.269, 0
590				0.118, 0	
611	0.29, 0	0.293, 0	0.201, 0	0.121, 0	0.259, 0
701	–	0.2, 0.035		0.101, 0	0.201, 0
729	0.185, 0	0.151, 0		0.132, 0	0.214, 0
793				0.064, 0	
863			0.119, 0	0.125, 0	0.146, 0
886	0.21, 0	0.233, 0	0.186, −0.029	0.156, 0	0.194, 0
917	0.11, 0	0.079, 0	0.16, 0		0.2, 0
979	0.355, 0	0.371, 0	0.34, 0	0.283, 0	0.336, 0
1004	0.135, 0			0.095, 0	
1072	0.125, 0	0.157, 0.038	0.17, 0	0.167, 0	0.16, 0
1103	0.08, 0		0.106, 0	0.124, 0	0.181, 0
1113	0.116, 0		0.16, 0	0.159, 0	0.195, 0
1168				0.126, 0.026	0.217, 0
1185	0.13, 0	0.185, 0	0.221, 0	0.227, 0	0.22, 0
1213	0.13, 0			0.074, 0	0.076, 0
1247		0.113, 0	0.117, 0	0.112, 0.021	0.142, 0
1264		0.102, 0		0.124, 0	0.142, 0
1308	0.242, 0	0.182, 0	0.17, 0	0.13, 0	0.149, 0
1348			0.117, 0	0.118, 0	0.155, 0
1388	0.095, 0				
1421	0.183, 0	0.098, 0		0.111, 0	0.093, −0.013
1506	0.2, 0		0.103, 0	0.115, 0	0.141, 0
1552	0.24, 0.046	0.211, −0.046	0.177, 0	0.147, 0	0.133, 0
1622	0.12, 0.017	0.179, 0	0.18, 0	0.20, −0.04	0.177, 0
1666	0.125, 0.033				
1689	0.204, 0.04	0.278, −0.062	0.321, 0	0.276, 0	0.252, 0
total vib. reorg. energy (λ_v)/cm^{-1} [c]	530	501	457	385	611

[a] See the Methods section and eqs 5−8 for description of parameters. [b] Actual vibrational frequencies in each solvent are given in Table 3. [c] Calculated as sum of $\omega\Delta^2/2$.

resonance Raman intensities in the limit of separable harmonic modes depend only on Δ^2, so for N Raman active modes, there are 2^N different sets of geometry changes equally consistent with the data.[28,40] PNA has only five or six strong resonance Raman lines, which were easily matched to the DFT-calculated normal modes, and the resulting 32 or 64 possible excited-state geometry changes were readily narrowed down to just a few that were deemed physically plausible. In the end, we were able to select a single sign combination, and thereby a single excited state geometry change in each solvent, that appeared significantly more likely than the others based on chemical reasonableness. For JTB, the total number of possible geometries is more than two million. Even if we assume that our ground-state normal mode assignments are *all* correct, which is unlikely, and apply reasonable constraints on the possible excited-state geometry changes (i.e., assuming that the directions of the bond length changes are what would be expected based on a more zwitterionic excited state), tens of thousands of sign combinations remain possible. Frequencies and intensities of isotopic derivatives would be helpful in both solidifying the ground-state vibrational assignments and defining the signs of the deltas, but a very large number of isotopomers would be needed to achieve anything close to a unique solution.[41−44]

Nevertheless, the solvent-dependent Δ values provide useful information even if we do not know in detail how they correspond to specific geometry changes. Relative to PNA, the displacements in JTB are much smaller; if we consider only the bending and stretching modes above 800 cm^{-1}, the maximum Δ values in PNA are about 1.5, about four times larger than those in JTB. To some degree, this difference merely reflects the larger number of modes among which the geometry changes are distributed in JTB, but the total vibrational reorganization energies (λ_v) are also larger in PNA than in JTB in the same solvent by factors of 3−4. This implies that the ground- and excited-state structures are more similar in JTB than in PNA, which would be interpreted within the two-state valence-bond models to mean that both ground and excited states are more nearly equal mixtures of neutral and zwitterionic basis states in JTB.

The reorganization energies due to classically behaved degrees of freedom (λ_s) are also found to be larger in PNA than in JTB by more than a factor of 10 in cyclohexane and by factors of 3−7 in the more polar solvents. Some of this reorganization may be attributable to unobserved low-frequency molecular modes in PNA, so the actual differences in *solvent* reorganization are probably not this large, but they do appear to be smaller

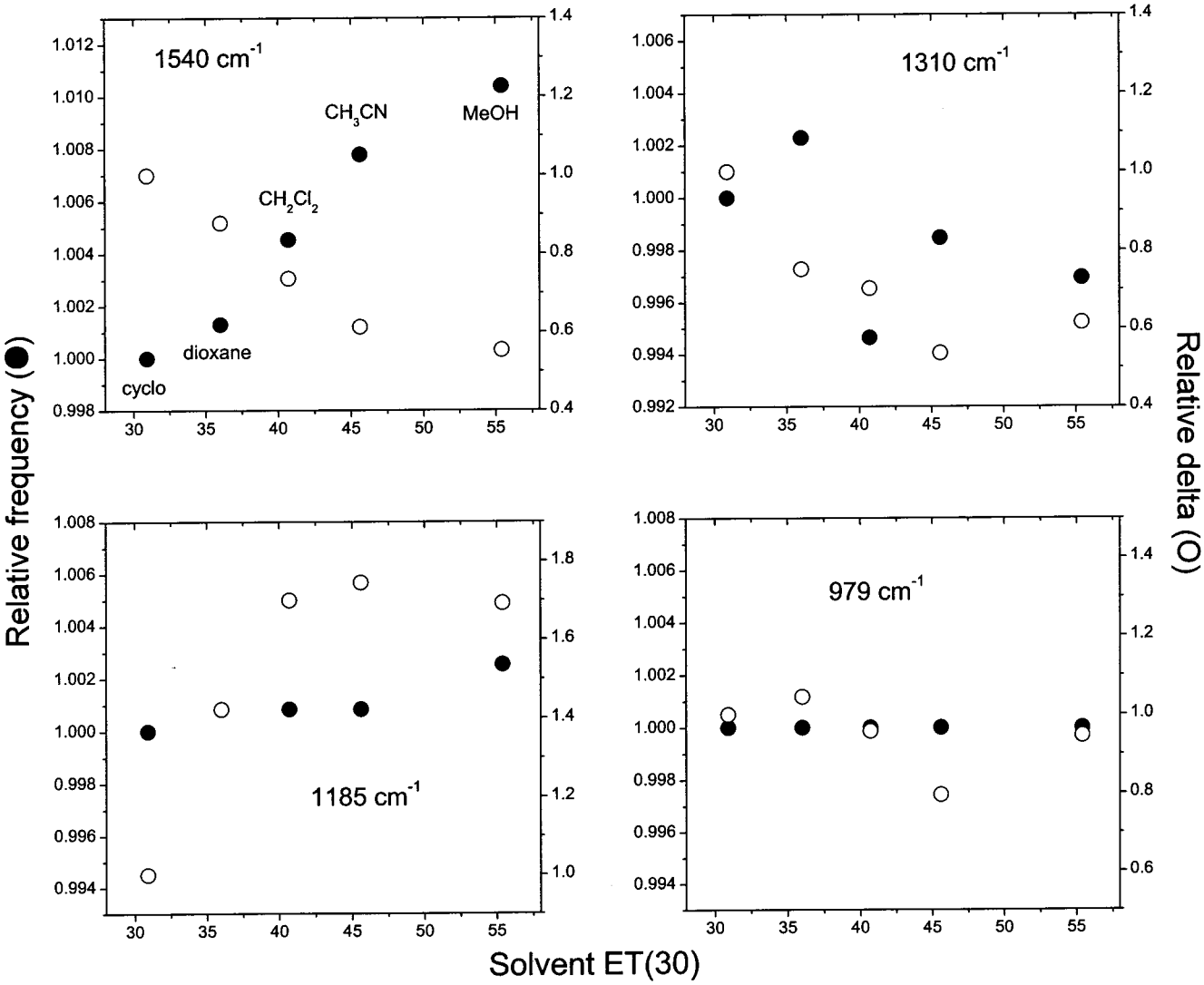

Figure 7. Frequency (solid circles) and displacement Δ (open circles) relative to cyclohexane for four vibrational modes of JTB as a function of solvent polarity parameter ET(30). The zeros of the *y* axes for different modes are different, but the ranges are the same for each mode: 0.015 for relative frequency and 1.0 for relative displacement.

in JTB than in PNA. For different probe molecules in the same solvent, the classical reorganization energy should depend on the square of the ground- to excited-state dipole moment change and inversely on the volume of the solvent cavity. The distance between the nitrogen donor and the center of the two oxygen acceptors in PNA is 6.2 Å, whereas the corresponding distance in JTB is 7.02 Å. The estimated volumes of PNA and JTB are about 300 and 870 Å^3, respectively. Therefore, if the same amount of charge is transferred in both molecules, the solvent reorganization energies should be only about 2.3 times larger in PNA than in JTB. This is a very crude estimate both because of the spherical cavity assumption and because the actual dipole moment change upon excitation of JTB is not known; as the ground state presumably has more zwitterionic character in JTB than in PNA, the effective amount of charge transferred upon excitation should be somewhat smaller in JTB. Nevertheless, these estimates seem to support the idea that only part of the apparent λ_s in PNA reflects true solvent contributions.

The model employed in the JTB spectral simulations differs in two respects from that used in our previous study of PNA. First, a contribution to the electronic line shape from pure exponential decay was introduced in order to better fit the tails of the absorption spectra on both low- and high-frequency sides. The Brownian oscillator used to model reorganization of the solvent and other classically behaved low-frequency modes gives a nearly Gaussian line shape in the slow modulation limit (small κ), and increasing κ leads to physically unrealistic parameters for the underlying oscillator.[31] The introduction of a purely exponential component (Lorentzian line shape) greatly improves the fits to the spectra. The Γ values of 100−175 cm^{-1} would correspond to lifetimes of 30−50 fs, which appear unreasonably short in view of the significant relaxed fluorescence observed, so this contribution to the line width should be attributed to some other, as yet undetermined process. In addition, some of the excitation profiles, particularly for some higher-frequency modes, could not be fit adequately without including a small coordinate dependence of the transition moment (non-Condon coupling). The electronic transition moment for an intramolecular charge-transfer transition should certainly have some dependence on the vibrational coordinates (i.e., the geometry), but this dependence is difficult to determine accurately from the data. A small nonzero $\partial\mu/\partial q$ in a particular mode changes the shape of the calculated excitation profile considerably without having much effect on the overall intensity of the profile. In view of the large variability in this parameter from one solvent to another (sometimes even changing sign), we consider this

TABLE 5: Experimental and Calculated Vibrational Frequencies and normal Modes for JTB

experimental			calculated (B3LYP/6-311G**)		
Raman[a] freq./cm^{-1}	IR[b] freq./cm^{-1}	IR int. (qual.)	freq./cm^{-1}	IR intensity	Normal mode description[c]
187			184		overall long-axis expansion
227			326		TBA NCS ip bend
367			373		TBA ip ring def
425			397		julol ip ring def
444			427		julol ip ring def/TBA ip ring def
495			463		expansion of julol top; C=O bend
573			548		TBA ip ring def
590			557		TBA/julol ip ring def
611			599		totally sym julol ip ring breathing
	668	w	681	2	julol/TBA ip ring def
700			711	8	julol/TBA ip ring def
729			741	5	delocalized skeletal bending
	783	w	794	26	TBA oop ring def
793			824	2	TBA ip ring def
863			868	3	TBA and phenyl ring defs
887			896	34	TBA sym ring def; phenyl ring def
917			930	12	julol CC str
	968	w	971	6	phenyl H oop
979	979	w	992	8	phenyl trigonal def
1000			1047	2	julol CC str
1072	sh.	vw	1084	29	julol CC str, TBA CC, CN str
	1085	w	1106	78	highly delocalized
1103	1104	s	1125	433	TBA ring str
1113			1133	25	TBA CN and CS str
1168	1165	m	1178	119	CC of linker; TBA asym C−C−C ring str
1185	1185	m	1205	496	delocalized ip str
1213	1216	w	1171	18	julolidine C−N str
1246			1263	59	TBA ring str
1264	1256	vs	1292	925	phenyl trigonal expansion, TBA CN str
1308	1309	s	1343	836	julol. CN str, TBA CN str
1346	1347	w	1368	102	phenyl CH rock
	∼1380 sh	w	1405	115	TBA ethyl CH_2
1388	1392	s	1421	982	TBA ring str
1421	1413	m	1451	204	TBA ring str, phenyl ring str, C=C and ethyl H rock
	1445	m	1469/1479	561/125	asym. quinoidal phenyl str/julol. CH_2 defs
1506	1499	s	1547	662	julol. CN str; CH_2 sym defs
1546			1571	524	C=C and C−C str of linker
1616	1612	w	1651	69	quinoidal julolidine sym str
1666	1654	m	1706	466	asym. C=O str
1689	1684	w	1738	120	sym. C=O str

[a] Solution phase; Raman frequencies are slightly solvent dependent (see text). [b] KBr pellet. [c] Abbreviations: TBA, thiobarbituric acid (acceptor group); julol, julolidine (donor group); ip, in-plane; oop, out-of-plane; str, stretch; def, deformation; sym, symmetric; asym, asymmetric.

quantity ill-defined by our fits and suggest that it not be taken too seriously. Setting all of the $\partial\mu/\partial q$ values to zero makes the calculated fits considerably worse but hardly changes the best-fit values of the excited-state displacements.

Simple theories of the coupling of electronic structure to geometry in conjugated push−pull systems typically assume the existence of a single "bond alternation coordinate", a delocalized stretching vibration of the whole molecule that lengthens the single bonds while shortening the double bonds.[45−47] The structural evolution from neutral to zwitterionic forms corresponds approximately to motion along this vibrational coordinate. Although the highest-frequency skeletal stretching mode of a simple linear polyene closely resembles this fictional bond alternation coordinate, there is no such vibration in JTB or many other real push−pull molecules, particularly those bearing aromatic groups that tend to disrupt the vibrational coupling across the molecule. The vibrational coordinate that takes JTB from its neutral to its zwitterionic form as shown in Figure 1 should involve the lengthening of the $C_{12}-C_{11}$, $C_{12}-C_{13}$, C_9-C_{14}, C_9-C_{10}, C_4-C_8, C_5-O_{21}, and C_3-O_{27} bonds and the shortening of the $N_{15}-C_{12}$, $C_{13}-C_{14}$, $C_{10}-C_{11}$, C_9-C_8, C_4-C_5, and C_4-C_3 bonds. The JTB vibration that comes closest to playing this role is the mode calculated at 1571 cm^{-1}, which we have assigned to the experimental frequency near 1546 cm^{-1}. This mode involves predominantly stretching of C_4-C_8 (the ethylenic double bond), with smaller contributions from the lengthening of $C_{13}-C_{12}$, C_9-C_{10}, C_5-O_{21}, and C_3-O_{27} and the shortening of C_9-C_8, $C_{13}-C_{14}$, and $C_{10}-C_{11}$. There is, however, one significant problem with this identification: the frequency of this mode increases with increasing solvent polarity, whereas we would expect it to decrease as the increasing ionicity reduces the bond order of the "double" bonds, particularly C_4-C_8. For polyene-like conjugated molecules such as retinal derivatives and cyanine dyes, it is well established that the frequencies of the nominally "double" bond stretches around 1500−1600 cm^{-1} decrease with increasing electron delocalization and concomitant red-shifting of the optical absorption.[48,49] In JTB, in contrast, none of the frequencies in the C=C stretching region decrease significantly as the absorption red-shifts, whereas at least two of them (the 1540 and 1616 cm^{-1} lines in cyclohexane) increase in frequency. The 1691 cm^{-1} line, assigned as predominantly the in-phase stretching of the two carbonyl groups, does shift to slightly lower frequencies with increasing solvent polarity as expected. What is less expected is the high resonance Raman intensity of this mode, as the stretching of the carbonyls is coupled to stretching of the C_8-C_9 single bond and shrinking

of the C_4-C_8 double bond, and the structural evolution toward a more zwitterionic form upon electronic excitation would not seem to have a large projection onto this mode.

The non- or counterintuitive solvent dependence of the ground-state vibrational frequencies indicates a deficiency in our understanding of the vibrational modes and/or the ground-state electronic structure of JTB. The increase with increasing solvent polarity of both the 1540 and 1616 cm^{-1} (in cyclohexane) frequencies would make sense if both modes have larger contributions from the quinoidal deformation of the julolidine phenyl group than from the ethylenic stretch. The vibrational coupling patterns in these push−pull molecules with aromatic groups may be sufficiently complex that one cannot straightforwardly predict how a given change in bond order will affect a particular frequency. Finally, the valence-bond structures depicted in Figure 1 may not be the most appropriate ones. For example, defining the zwitterionic state to have the positive charge delocalized over the julolidine group and/or the negative charge delocalized over the thiobarbituric acid group would lead to somewhat different expected bond order changes. Of course, many valence-bond resonance structures can be drawn for JTB, and if a large number of these are needed to adequately describe the electronic states, a two-state valence-bond model is not appropriate. It may, however, be possible to obtain a better description of the states within a two-state model by defining the states differently from those implied by Figure 1.

A final complication that might enter into the interpretation of these experiments is the possibility of torsional heterogeneity or solvent-dependent torsional angles. Figure 1 as drawn suggests considerable steric hindrance between O_{21} and the hydrogen on C_{14}. This could be relieved by twisting about the C_8-C_9 and/or C_4-C_8 bonds, at the cost of some loss of conjugation, and/or by opening up the CCC bond angle of the ethylenic linker. Our DFT calculations give a nearly planar equilibrium geometry with the $C_{14}C_9C_8C_4$ and $C_9C_8C_4C_5$ dihedral angles both less than 1°, but a very large distortion in the $C_4C_8C_9$ bond angle to 139°. DFT calculations with the B3LYP functional generally tend to overestimate electron delocalization, suggesting that the true structure might be more torsionally distorted than calculated, or at least that there may be a wide range of torsional angles present in solution. (We do note, however, that the calculated dipole moment of 10.1 D is in reasonable agreement with the experimental value of 8.25 D measured in toluene solution.[24]) A range of torsional angles in methanol might explain the variation in the frequency of the 186 cm^{-1} mode with excitation frequency and the increased amount of electronic inhomogeneous broadening required to model the profiles in this solvent. Excitation wavelength dependent resonance Raman frequencies for some high-frequency modes were recently observed in phenol blue[50] and attributed to an inhomogeneous distribution of ground-state solvation structures, not torsional coordinates.[51] The ground and excited electronic states are almost certain to have different torsional minima if they are nonplanar, which should lead to significant resonance Raman activity in out-of-plane vibrations. Strong hydrogen out-of-plane wagging activity, in particular, is a hallmark of severely nonplanar ground-state geometries in conjugated molecules such as *cis*-stilbene[52] and bathorhodopsin.[53] Our normal mode assignments are not accurate enough to allow us to exclude this possibility; for example, the very strong Raman line at 979 cm^{-1}, assigned here as predominantly an in-plane phenyl deformation, is also in the expected frequency region for the ethylenic hydrogen out-of-plane wag, and the strong 186 cm^{-1} mode could also reasonably be assigned as an out-of-plane skeletal vibration. Spectra of isotopic derivatives would be helpful in resolving this question.

Conclusions

Quantitative modeling of the absorption spectra and resonance Raman excitation profiles of JTB shows that the internal vibrational reorganization energy decreases with increasing solvent polarity in solvents that are not strongly hydrogen-bonding. This result is qualitatively consistent with two-state valence-bond models which predict increased mixing of the neutral and zwitterionic diabatic basis states into the ground and excited adiabatic electronic states as solvent polarity increases. However, the solvent-dependent ground-state frequencies appear inconsistent with the expectation of increased ground-state bond-order alternation in more polar solvents. The component of the solvent reorganization energy that is fast on the time scale of ground-state vibrational dephasing increases with increasing solvent polarity except in methanol, which shows smaller solvent and larger vibrational reorganization energies and a greater amount of electronic inhomogeneous broadening. These results may reflect a distribution of slowly interconverting solvent−solute structures in the hydrogen-bonding solvent.

Acknowledgment. This work was supported in part by ACS-PRF Grant 33963-AC6 and NSF Grant CHE-9708382. We thank Professor Paul Baures for the use of his FTIR spectrometer and Professor Debra Egolf for making some of the solvent cross section measurements.

References and Notes

(1) Albert, I. D. L.; Marks, T. L.; Ratner, M. A. *J. Phys. Chem.* **1996**, *100*, 9714−9725.

(2) Kanis, D. R.; Ratner, M. A.; Marks, T. J. *Chem. Rev.* **1994**, *94*, 195−242.

(3) Lu, D.; Marten, B.; Cao, Y.; Ringnalda, M. N.; Friesner, R. A.; Goddard, W. A., III. *Chem. Phys. Lett.* **1995**, *242*, 543−547.

(4) Marder, S. R.; Beratan, D. N.; Cheng, L.-T. *Science* **1991**, *252*, 103−106.

(5) Marder, S. R.; Cheng, L.-T.; Tiemann, B. G.; Friedli, A. C.; Blanchard-Desce, M.; Perry, J. W.; Skindhøj, J. *Science* **1994**, *263*, 511−514.

(6) Prasad, N. P.; Williams, D. J. *Introduction to Nonlinear Optical Effects in Molecules and Polymers*; Wiley: New York, 1991.

(7) Shu, Y.-C.; Gong, Z.-H.; Shu, C.-F.; Breitung, E. M.; McMahon, R. J.; Lee, G.-H.; Jen, A. K.-Y. *Chem. Mater.* **1999**, *11*, 1628−1632.

(8) Thayumanavan, S.; Mendez, J.; Marder, S. R. *J. Org. Chem.* **1999**, *64*, 4289−4297.

(9) *Molecular Nonlinear Optics: Materials, Physics, and Devices*; Zyss, J., Ed.; Academic Press: Boston, MA, 1993.

(10) Rojo, G.; Agulló-López, F.; Cabezón, B.; Torres, T.; Brasselet, S.; Ledoux, I.; Zyss, J. *J. Phys. Chem. B* **2000**, *104*, 4295−4299.

(11) Zyss, J.; Ledoux, I.; Volkov, S.; Chernyak, V.; Mukamel, S.; Bartholomew, G. P.; Bazan, G. C. *J. Am. Chem Soc.* **2000**, *122*, 11956−11962.

(12) Ma, H.; Chen, B.; Sassa, T.; Dalton, L. R.; Jen, A. K.-Y. *J. Am. Chem Soc.* **2001**, *123*, 986−987.

(13) Bishop, D. M.; Champagne, B.; Kirtman, B. *J. Chem. Phys.* **1998**, *109*, 9987−9994.

(14) Blanchard-Desce, M.; Barzoukas, M. *J. Opt. Soc. Am. B* **1998**, *15*, 302−307.

(15) Chen, G.; Lu, D.; Goddard, W. A., III. *J. Chem. Phys.* **1994**, *101*, 5860−5864.

(16) Lu, D.; Chen, G.; Perry, J. W.; Goddard, W. A., III. *J. Am. Chem. Soc.* **1994**, *116*, 10679−10685.

(17) Thompson, W. H.; Blanchard-Desce, M.; Hynes, J. T. *J. Phys. Chem. A* **1998**, *102*, 7712−7722.

(18) Thompson, W. H.; Blanchard-Desce, M.; Alain, V.; Muller, J.; Fort, A.; Barzoukas, M.; Hynes, J. T. *J. Phys. Chem. A* **1999**, *103*, 3766−3771.

(19) Painelli, A. *Chem. Phys.* **1999**, *245*, 185−197.

(20) Painelli, A.; Terenziani, F. *J. Phys. Chem. A* **2000**, *104*, 11041−11048.

(21) Cho, M. *J. Phys. Chem. A* **1998**, *102*, 703−707.

(22) Plaza, P.; Laage, D.; Martin, M. M.; Alain, V.; Blanchard-Desce, M.; Thompson, W. H.; Hynes, J. T. *J. Phys. Chem. A* **2000**, *104*, 2396−2401.
(23) Moran, A. M.; Kelley, A. M. *J. Chem. Phys.* **2001**, *115*, 912−924.
(24) Blanchard-Desce, M.; Alain, V.; Bedworth, P. V.; Marder, S. R.; Fort, A.; Runser, C.; Barzoukas, M.; Lebus, S.; Wortmann, R. *Chem. Eur. J.* **1997**, *3*, 1091−1104.
(25) Stähelin, M.; Burland, D. M.; Rice, J. E. *Chem. Phys. Lett.* **1992**, *191*, 245−250.
(26) Rechthaler, K.; Köhler, G. *Chem. Phys. Lett.* **1996**, *250*, 152−158.
(27) *Advances in Organic Chemistry: Methods and Results*; Raphael, R. A., Ed.; Interscience: New York, 1976; Vol. 9, p 225.
(28) Myers, A. B. In *Laser Techniques in Chemistry*; Myers, A. B., Rizzo, T. R., Eds.; Wiley: New York, 1995; pp 325−384.
(29) Lilichenko, M.; Tittelbach-Helmrich, D.; Verhoeven, J. W.; Gould, I. R.; Myers, A. B. *J. Chem. Phys.* **1998**, *109*, 10958−10969.
(30) The dimensionless normal coordinate q_j corresponding to the normal mode with angular frequency ω_j and reduced mass μ_j is defined as $q_j = \sqrt{\mu_j \omega_j / \hbar} Q_j$ where Q_j is the normal coordinate in units of Å. $Q_j = \sum_{i=1}^{3N} L_{ji} X_i$ where X_i is the displacement along the ith Cartesian coordinate in normal mode j, and the L_{ji} are the Cartesian normal mode coefficients. Δ is the displacement in dimensionless coordinates between excited and ground-state potential minima along a particular normal mode. $\Delta = 1$ is a displacement equal to one standard deviation of the Gaussian $n = 0$ vibrational wave function.
(31) Li, B.; Johnson, A. E.; Mukamel, S.; Myers, A. B. *J. Am. Chem. Soc* **1994**, *116*, 11039−11047.
(32) Mukamel, S. *Principles of Nonlinear Optical Spectroscopy*; Oxford University Press: New York, 1995.
(33) Frisch, M. J.; Trucks, G. W.; Schlegel, H. B.; Scuseria, G. E.; Robb, M. A.; Cheeseman, J. R.; Zakrzewski, V. G.; Montgomery, J. A., Jr.; Stratmann, R. E.; Burant, J. C.; Dapprich, S.; Millam, J. M.; Daniels, A. D.; Kudin, K. N.; Strain, M. C.; Farkas, O.; Tomasi, J.; Barone, V.; Cossi, M.; Cammi, R.; Mennucci, B.; Pomelli, C.; Adamo, C.; Clifford, S.; Ochterski, J.; Petersson, G. A.; Ayala, P. Y.; Cui, Q.; Morokuma, K.; Malick, D. K.; Rabuck, A. D.; Raghavachari, K.; Foresman, J. B.; Cioslowski, J.; Ortiz, J. V.; Stefanov, B. B.; Liu, G.; Liashenko, A.; Piskorz, P.; Komaromi, I.; Gomperts, R.; Martin, R. L.; Fox, D. J.; Keith, T.; Al-Laham, M. A.; Peng, C. Y.; Nanayakkara, A.; Gonzalez, C.; Challacombe, M.; Gill, P. M. W.; Johnson, B. G.; Chen, W.; Wong, M. W.; Andres, J. L.; Head-Gordon, M.; Replogle, E. S.; Pople, J. A. *Gaussian 98*, revision A.7; Gaussian, Inc.: Pittsburgh, PA, 1998.
(34) Trulson, M. O.; Mathies, R. A. *J. Chem. Phys.* **1986**, *84*, 2068−2074.
(35) *CRC Handbook of Chemistry and Physics*, 73rd ed.; Chemical Rubber Company: Boca Raton, FL, 1992.
(36) Reichardt, C. *Chem. Rev.* **1994**, *94*, 2319−2358.
(37) Moran, A. M. Unpublished results.
(38) Kelley, A. M. Unpublished results.
(39) Moran, A. M.; Egolf, D. S.; Blanchard-Desce, M.; Kelley, A. M. *J. Chem. Phys.* Submitted for publication.
(40) Myers, A. B.; Mathies, R. A. In *Biological Applications of Raman Spectroscopy*; Spiro, T. G., Ed.; Wiley: New York, 1987; Vol. 2; pp 1−58.
(41) Phillips, D. L.; Myers, A. B. *J. Raman Spectrosc.* **1997**, *28*, 839−848.
(42) Baranovic, G. *J. Raman Spectrosc.* **2001**, *32*, 293−299.
(43) Myers, A. B. Ph.D. Thesis, University of California, Berkeley, 1984.
(44) Wright, P. G.; Stein, P.; Burke, J. M.; Spiro, T. G. *J. Am. Chem. Soc.* **1979**, *101*, 3531−3535.
(45) Del Zoppo, M.; Castiglioni, C.; Gerola, V.; Zuliani, P.; Zerbi, G. *J. Opt. Soc. Am. B* **1998**, *15*, 308−317.
(46) Zuliani, P.; Del Zoppo, M.; Castiglioni, C.; Zerbi, G.; Marder, S. R.; Perry, J. W. *J. Chem. Phys.* **1995**, *103*, 9935−9940.
(47) Gorman, C. B.; Marder, S. R. *Chem. Mater.* **1995**, *7*, 215−220.
(48) Callender, R.; Honig, B. *Annu. Rev. Biophys. Bioeng.* **1977**, *6*, 33−55.
(49) Kochendoerfer, G. G.; Wang, Z.; Oprian, D. D.; Mathies, R. A. *Biochemistry* **1997**, *36*, 6577−6587.
(50) Yamaguchi, T.; Kimura, Y.; Hirota, N. *J. Chem. Phys.* **1998**, *109*, 9075−9083.
(51) Yamaguchi, T.; Kimura, Y.; Hirota, N. *J. Chem. Phys.* **1998**, *109*, 9084−9095.
(52) Myers, A. B.; Mathies, R. A. *J. Chem. Phys.* **1984**, *81*, 1552−1558.
(53) Mathies, R. A.; Smith, S. O.; Palings, I. In *Biological Applications of Raman Spectroscopy*; Spiro, T. G., Ed.; John Wiley & Sons: New York, 1987; Vol. 2; pp 59−108.